CHALMERS
UNIVERSITY OF TECHNOLOGY

Analysis of nonlinearity mitigation using phase-sensitive optical parametric amplifiers

Research Article | Vol. 27, No. 22 / 28 October 2019 / Optics Express 31926
Optics EXPRESS

Analysis of nonlinearity mitigation using phase-sensitive optical parametric amplifiers

BENJAMIN FOO,[1,2] MAGNUS KARLSSON,[1] KOVENDHAN VIJAYAN,[1] MIKAEL MAZUR,[1] AND PETER A. ANDREKSON[1,*]

[1] *Photonics Laboratory, Deptartment of Microtechnology and Nanoscience (MC2), Chalmers University of Technology, SE-412 96, Gothenburg, Sweden*
[2] *Now with Infinera Corporation, 7360 Windsor Drive, Allentown, PA, 18106, USA*
[*] *peter.andrekson@chalmers.se*

Abstract: Phase-sensitive optical parametric amplifiers (PSAs) can provide low-noise optical amplification while simultaneously mitigating nonlinear distortions caused by the Kerr effect. However, nonlinearity mitigation using PSAs is affected by link parameters, and imperfect link design results in residual nonlinear distortions. In this paper, we use first-order perturbation theory to describe these residual nonlinear distortions, and develop a way to mitigate them using a modified third-order Volterra nonlinear equalizer (VNLE) in the receiver. Using numerical simulations, we show that our proposed VNLE reduces the residual nonlinear distortions in links using in-line PSAs for several combinations of symbol rates and modulation formats, and can increase the maximum transmission distance by up to 80%. We also perform a proof-of-concept experiment and confirm that our modified VNLE can mitigate the residual nonlinear distortions on a 10-Gbaud 16QAM signal after transmission through a 10×80-km link with in-line PSAs.

1. Introduction

The transmission performance of modern long-haul optical communications systems is limited by additive white Gaussian noise (AWGN) from optical amplifiers and distortions caused by the nonlinear Kerr effect [1–3]. AWGN places a fundamental limit on the capacity of any linear communications channel [4], and can generally be overcome by increasing the signal power. However, the optical fiber channel is nonlinear, and increasing the signal power causes systems to run into the limitation imposed by the Kerr effect [1]. Physically, the nonlinear Kerr effect is a change in the refractive index of the optical fiber that depends on the instantaneous power of the signal [5]. As this is a deterministic effect, distortions from the Kerr nonlinearity can be compensated with sufficient information about the link and the transmitted signal. This has led to the development of various nonlinearity compensation (NLC) techniques in both the digital [6–9], and optical [10–12] domains.

One way to simultaneously combat AWGN and fiber nonlinearity is to use phase-sensitive optical parametric amplifiers (PSAs). In general, parametric amplifiers utilize the nonlinear response of a material to transfer energy from a high-power 'pump' to the 'signal' that is being amplified [13]. In a PSA, the gain also depends on the relative phase between the pump, signal, and a third input, commonly referred to as the 'idler', that is related to the signal. The exact phase relationship between these three inputs determines whether a PSA amplifies the signal or attenuates it [14]. Due to this property, PSAs have been used for a variety of optical signal processing applications, such as all-optical phase and amplitude regeneration [15], quadrature de-multiplexing [16], and enhanced optical filtering [17].

In the context of fiber transmission, PSAs are an interesting research area as they provide a way to achieve low-noise optical amplification. While phase-insensitive amplifiers, e.g. Erbium-doped fiber amplifiers (EDFAs), have a theoretical quantum-limited noise figure (NF) of 3 dB in the high-gain regime, a phase-sensitive amplifier can achieve a quantum-limited NF of 0 dB [18].

#372384 https://doi.org/10.1364/OE.27.031926
Journal © 2019 Received 12 Jul 2019; revised 11 Sep 2019; accepted 12 Sep 2019; published 18 Oct 2019

Optics EXPRESS

PSAs with NFs below the 3-dB limit have been demonstrated experimentally in both χ^2 and χ^3 nonlinear media [19,20]. Additionally, PSAs deployed using the copier-PSA scheme [21] can mitigate the distortions caused by the nonlinear Kerr effect when the idler is the phase conjugate of the signal [22]. In a recent experimental demonstration, the combined effects of low-noise optical amplification and NLC when using in-line PSAs enabled a significant increase in the maximum transmission distance of a long-haul optical communications link [23]. However, because the information on the signal and idler are related, the spectral efficiency of a link that uses in-line PSAs is reduced by a factor of two.

While low-noise amplification using PSAs has been explored both theoretically [18,24] and experimentally [19,20,25,26], the nonlinearity mitigation aspect of PSAs is less well understood. Conceptually, nonlinearity mitigation using PSAs is very similar to the phase-conjugate twin wave (PCTW) technique proposed by Liu *et al.* [27,28]. This approach can cancel nonlinear distortions, to first order, but is very sensitive to link design and requires the use of distributed amplification for maximum effectiveness. While several previous studies have considered how the link parameters [29–32] and optical signal bandwidth [32,33] affect the efficacy of NLC using PSAs, to the best of the authors' knowledge, there has not been a detailed investigation of the underlying reasons for the trends observed in those studies. We aim to address this issue with the current work.

We start by combining the matrix description of a parametric amplifier [24] with the first-order solution of the perturbation approach [34] to obtain an expression for the signal after NLC using a PSA. This analysis reveals that PSAs generally do not fully compensate the nonlinear distortion, and shows how the magnitude of the residual nonlinear distortion can be reduced by optimizing the link parameters. We then propose adding a Volterra nonlinear equalizer (VNLE) using a modified third-order kernel to the receiver-side digital signal processing (DSP) chain to remove the residual distortion. A similar approach combining a modified VNLE with optical phase conjugation was recently studied by Saavedra *et al*. [35]. We perform numerical simulations for a variety of link conditions to assess the efficacy of the proposed VNLE. These simulations indicate that links employing in-line PSAs suffer significant performance penalties due to residual nonlinear distortions, and that these penalties can be greatly reduced using our modified VNLE. Applying our modified VNLE to an optimized link using in-line PSAs can increase the achievable transmission distance by up to 80%. Finally, we validate our findings using a proof-of-concept re-circulating loop experiment, which was originally reported in [36], and confirm that our proposed VNLE can remove the residual nonlinear distortions present on a 10-Gbaud 16-ary quadrature amplitude modulation (16QAM) signal after transmission through a link with ten 80-km spans and in-line PSAs.

The remainder of this paper is structured as follows: in Section 2 we present a first-order perturbation analysis of nonlinearity mitigation using in-line PSAs, which produces an equation for the residual nonlinear distortion. We then describe how to modify the third-order Volterra kernel to create a VNLE to undo this residual distortion. In Section 3 we evaluate the effectiveness of our modified VNLE using numerical simulations, and verify these results with a proof-of-concept experiment in Section 4. Section 5 discusses several aspects of using in-line PSAs for NLC, and the paper concludes with Section 6.

2. Nonlinearity mitigation using the copier-PSA scheme

Assuming no pump depletion, the output of a two-mode, degenerate pump fiber optic parametric amplifier (FOPA) can be described using the matrix equation [24]:

$$\begin{bmatrix} B_s(\omega) \\ B_i^*(-\omega) \end{bmatrix} = \begin{bmatrix} \mu & \nu \\ \nu^* & \mu^* \end{bmatrix} \begin{bmatrix} A_s(\omega) \\ A_i^*(-\omega) \end{bmatrix}$$

Optics EXPRESS

,where ω is the angular frequency, $A(\omega)$ and $B(\omega)$ describe the complex fields in the frequency domain at the input and output of the FOPA, respectively, and $(.)^*$ represents the phase conjugate operation. The $-\omega$ terms are the result of the conjugation property of the Fourier transform, and the subscripts s and i, respectively, refer to the signal and idler. The complex coefficients μ and ν describe the parametric gain experienced by the signal and conversion efficiency of the idler, respectively, and are constrained by $|\mu|^2 - |\nu|^2 = 1$ to satisfy the Manley-Rowe invariant [14]. The exact expressions of μ and ν for a FOPA can be found in [24], but are not important for this discussion.

For a phase-insensitive FOPA, only the signal is present at the input, and so its outputs are:

$$B_{\mathrm{PI,\,s}}(\omega) = \mu A_s(\omega), \quad \text{and} \quad B_{\mathrm{PI,\,i}}(\omega) = \nu A_s^*(-\omega), \tag{2}$$

which means that the gain of the phase-insensitive FOPA is $G_{\mathrm{PI}} = |\mu|^2$. Additionally, Eq. (2) shows that the idler generated by a phase-insensitive FOPA is related to the phase conjugate of the input signal, which will be useful in our discussion of the copier-PSA scheme.

For phase-sensitive FOPAs, both signal and idler are present at the input, and so the outputs are

$$B_{\mathrm{PS,\,s}}(\omega) = \mu A_s(\omega) + \nu A_i^*(-\omega) \quad \text{and} \quad B_{\mathrm{PS,\,i}}(\omega) = \mu A_i(\omega) + \nu A_s^*(-\omega), \tag{3}$$

meaning that the field of the signal is coherently added to the phase conjugated field of the idler. When the input signal and idler have the same power, the gain of a phase-sensitive FOPA is [14]:

$$G_{\mathrm{PS}}(\theta_{\mathrm{rel}}) = |\mu|^2 + |\nu|^2 + 2|\mu||\nu|\cos(\theta_{\mathrm{rel}}), \tag{4}$$

where $\theta_{\mathrm{rel}} = \theta_{\mathrm{s}} + \theta_{\mathrm{i}} - 2\theta_{\mathrm{p}}$ is the relative phase of the pump, signal, and idler at the input of the PSA. This dependence of G_{PS} on θ_{rel} is why this type of amplifier is called 'phase-sensitive', and the gain is maximized when $\theta_{\mathrm{rel}} = 0$. Therefore, the maximum phase-sensitive gain is $G_{\mathrm{PS,\,max}} = (|\mu| + |\nu|)^2$, meaning that in the high-gain regime ($|\mu|^2 >> 1$), $G_{\mathrm{PS,\,max}} \approx 4G_{\mathrm{PI}}$. Assuming that the phase-insensitive gain is large and that the phases of the interactive waves are tuned to maximize the phase-sensitive gain, it is useful to adopt the approximations [29]:

$$B_{\mathrm{PS,\,s}}(\omega) \approx |\mu|(A_s(\omega) + A_i^*(-\omega)) \quad \text{and} \quad B_{\mathrm{PS,\,i}}(\omega) \approx |\mu|(A_i(\omega) + A_s^*(-\omega)), \tag{5}$$

to describe the output of a PSA.

In the special case when the idler is the phase conjugate of the signal, i.e. $A_i(\omega) = A_s^*(-\omega)$, a PSA will amplify both in-phase and quadrature components of the signal when the gain is maximized [29]. As shown by Eq. (2), the required idler can be generated using a phase-insensitive FOPA, which is the 'copier' in the copier-PSA scheme [21]. An illustration of a copier-PSA transmission link is shown in Fig. 1, which consists of the copier, a span of standard single-mode fiber (SSMF), the PSA, and two dispersion compensating modules (DCMs). The signal and idler fields are marked at different points to show the impact of different transmission effects. During transmission, the signal will be affected by attenuation, chromatic dispersion, and the Kerr nonlinearity. Attenuation reduces the power of the signal, and we assume that the span loss is perfectly compensated by the gain provided by the PSA. In this case, the fiber span will reduce the signal power by a factor of $4G_{\mathrm{PI}}$. Chromatic dispersion can be described in the frequency domain by multiplying $E_{s/i}(\omega)$ by $\exp(j\beta_2\omega^2 L_{\mathrm{span}}/2)$, where L_{span} and β_2 are the length and group velocity dispersion (GVD) parameter of the SSMF span, respectively, and $j = \sqrt{-1}$. If there is non-zero chromatic dispersion at the input to the PSA, the idler is no longer the phase conjugate of the signal. As a result, G_{PS} varies with wavelength, and this effect has been utilized to demonstrate simultaneous phase-sensitive amplification and attenuation using the copier-PSA scheme [21]. However, such behavior is undesirable in the current application, and so dispersion is fully compensated before the PSA using optical DCMs. These DCMs apply

Optics EXPRESS

a combination of pre-compensation, D_0, and post-compensation, D_1, such that the sum of the pre- and post-compensation modules perfectly compensates the total dispersion accumulated over the span, i.e., $D_0 + D_1 = -\beta_2 L_{\text{span}}/2$. The impact of the Kerr effect is more difficult to describe accurately, and generally requires solving the Nonlinear Schrödinger equation (NLSE) numerically. A previous study [29] considered the distortion as a power-dependent phase rotation, though that approximation does not consider the interaction between dispersion and the Kerr nonlinearity. A more accurate description of a transmission system assumes that the fiber is weakly nonlinear, and that the nonlinear distortion introduces a small perturbation to the linear solution. In this case, the output of a fiber span after compensating for dispersion and attenuation is [34]:

$$E'_{s/i}(\omega) = E_{s/i}(\omega) + \delta_{\text{NL},s/i}(\omega), \tag{6}$$

where $\delta_{\text{NL}s/i}(\omega)$ is the small perturbation representing the nonlinear distortion on the signal or idler. Applying the span loss to the signal and idler described by Eq. (6) and substituting the result into Eq. (5), the signal at the output of a PSA can be found as:

$$\begin{aligned} E_{\text{PSA},s}(\omega) &= |\mu| \left(\frac{E'_s(\omega)}{2|\mu|} + \frac{E'^*_i(-\omega)}{2|\mu|} \right) \\ &= E_s(\omega) + 0.5 \left(\delta_{\text{NL},s}(\omega) + \delta^*_{\text{NL},i}(-\omega) \right). \end{aligned} \tag{7}$$

Adding the nonlinear perturbations experienced by the signal and idler can partially cancel the nonlinear distortion [27], and the fraction of the nonlinear distortion that is not cancelled by the PSA is the residual nonlinear distortion, $\delta_{\text{NL, res}}(\omega) = 0.5 \left(\delta_{\text{NL},s}(\omega) + \delta^*_{\text{NL},i}(-\omega) \right)$.

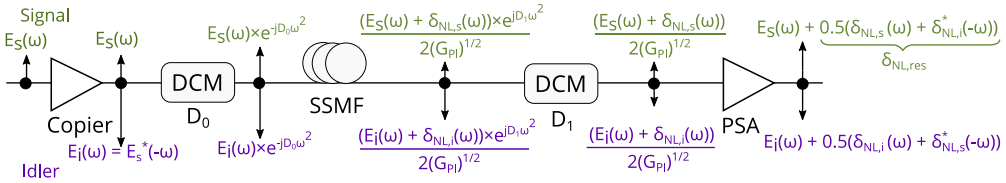

Fig. 1. Illustration of a copier-PSA link with the signal and idler fields marked at several points. We assume that the PSA perfectly compensates the span loss and that the effect of the Kerr nonlinearity is described as a small perturbation to the output of a linear channel. Abbreviations are explained in the text.

As a first-order approximation, the nonlinear perturbation at the end of a span with length L_{span} is [34]:

$$\delta_{\text{NL}}(\omega, L_{\text{span}}) = j\gamma \int_{-\infty}^{\infty} \int_{-\infty}^{\infty} \eta(\Delta\Omega, L_{\text{span}}) E(\omega_1, 0) E^*(\omega_2, 0) E(\omega - \omega_1 + \omega_2, 0) d\omega_1 d\omega_2, \tag{8}$$

where $E(\omega, 0)$ is the Fourier transform of the electric field at the start of the span, and $\eta(\Delta\Omega, L_{\text{span}})$ is the span transfer function:

$$\eta(\Delta\Omega, L_{\text{span}}) = \int_0^{L_{\text{span}}} \exp(G(z) + j\Delta\Omega D(z)) dz, \tag{9}$$

where G(z) is the evolution of the signal amplitude, and D(z) describes how dispersion accumulates along the span. Integrating ω_1 and ω_2 from $-\infty$ to ∞ indicates that Eq. (8) is the summation of all possible four-wave mixing products between spectral components at ω_1, ω_2, and $\omega_3 = \omega - \omega_1 + \omega_2$ that distort the field at angular frequency ω. Formally, these limits are independent of the

Optics EXPRESS

modulation format and symbol rate, and so we will drop them in future equations for compactness. The frequency difference between the four interacting tones, $\Delta\Omega = (\omega_1 - \omega)(\omega_1 - \omega_2)$, leads to a group velocity mismatch described by $\beta_2\Delta\Omega$, which affects the strength of the four-wave mixing product. For the copier-PSA link in Fig. 1, which does not include distributed amplification and applies the dispersion pre-compensation D_0, the span transfer function is [34]:

$$\begin{aligned}\eta(\Delta\Omega, L_{\text{span}}) &= \int_0^{L_{\text{span}}} \exp(-\alpha z + j\Delta\Omega(\beta_2 z - D_0))dz, \\ &= \frac{1 - \exp(-\alpha L_{\text{span}} + j\Delta\Omega\beta_2 L_{\text{span}})}{\alpha - j\Delta\Omega\beta_2}\exp(-j\Delta\Omega D_0),\end{aligned} \tag{10}$$

where α and β_2 are the attenuation and GVD of the fiber, respectively. If we assume that the span transfer functions for the signal and idler are approximately the same, we can use the relationship $E_i(\omega, 0) = E_s^*(-\omega, 0)$ to the find the residual nonlinear distortion [28]:

$$\begin{aligned}\delta_{\text{NL,res}}(\omega, L_{\text{span}}) = 0.5j\gamma\Bigg(&\int\int \eta(\Delta\Omega, L_{\text{span}})E_s(\omega_1, 0)E_s^*(\omega_2, 0)E_s(\omega - \omega_1 + \omega_2, 0)d\omega_1 d\omega_2 \\ &- \int\int \eta^*(\Delta\Omega, L_{\text{span}})E_i^*(-\omega_1, 0)E_i(-\omega_2, 0)E_i^*(\omega_1 - \omega_2 - \omega, 0)d\omega_1 d\omega_2\Bigg) \\ = j\gamma &\int\int \eta_{\text{res}}(\Delta\Omega, L_{\text{span}})E_s(\omega_1, 0)E_s^*(\omega_2, 0)E_s(\omega - \omega_1 + \omega_2, 0)d\omega_1 d\omega_2,\end{aligned} \tag{11}$$

remembering that $E_i(\omega) = E_s^*(-\omega)$ and where:

$$\begin{aligned}\eta_{\text{res}}(\Delta\Omega, L_{\text{span}}) &= 0.5(\eta(\Delta\Omega, L_{\text{span}}) - \eta^*(\Delta\Omega, L_{\text{span}})) \\ &= j\text{Im}\left\{\frac{1 - \exp(-\alpha L_{\text{span}} + j\Delta\Omega\beta_2 L_{\text{span}})}{\alpha - j\Delta\Omega\beta_2}\exp(-j\Delta\Omega D_0)\right\},\end{aligned} \tag{12}$$

is the effective transfer function of the signal after NLC using a PSA. Equation (14) shows that the coherent superposition in a PSA cancels the nonlinear distortions caused by the real part of $\eta(\Delta\Omega, L_{\text{span}})$, but not the distortions from the imaginary part. This failure to cancel part of the nonlinear distortion is the underlying reason why the NLC provided by a PSA depends on the link parameters and signal bandwidth. From inspection, Eq. (14) includes terms for the fiber attenuation and GVD, clearly demonstrating that the nonlinearity mitigation depends on the link parameters. Further, the last exponential term on the right-hand side of Eq. (14) indicates that the strength of the residual distortion depends on the amount of dispersion pre-compensation, and the optimization of this parameter has been explored extensively [29,30,32]. Additionally, each value of $\Delta\Omega$ requires a slightly different value of D_0 to minimize Eq. (14), which means that the magnitude of the residual distortion depends on the range of values that ω_1 and ω_2 can take where both $E_s(\omega_1, 0)$ and $E_s(\omega_2, 0)$ are non-zero, i.e., the bandwidth of the optical signal. As a result, PSAs are less effective at mitigating the nonlinear distortion for signals with larger optical bandwidths, and this effect has been observed experimentally [33] and in numerical simulations [32].

We can extend this analysis to a multi-span link with in-line PSAs by coherently summing the nonlinear perturbations from each span [34]. Assuming the same amount of dispersion pre-compensation in every span and that the total residual nonlinear distortion at the end of the link still a small perturbation of the linear solution, the output at the end of a link with N_{span} spans is:

$$E_s(\omega, N_{\text{span}}L_{\text{span}}) = E_s(\omega, 0) + N_{\text{span}}\delta_{\text{NL,res}}(\omega, L_{\text{span}}). \tag{13}$$

This indicates that the residual nonlinear distortion accumulates linearly with the number of spans.

Optics EXPRESS

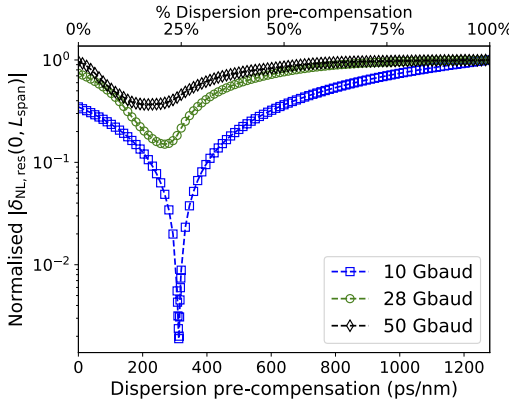

Fig. 2. The magnitude of $\delta_{\mathrm{NL,\,res}}(0, L_{\mathrm{span}})$ vs. dispersion pre-compensation for 10- (squares), 28- (circles), and 50-Gbaud (diamonds) signals. Curves are normalized to the maximum residual distortion for each symbol rate.

We illustrate how dispersion pre-compensation and optical signal bandwidth affect nonlinearity mitigation by plotting $\delta_{\mathrm{NL,\,res}}(0, L_{\mathrm{span}})$ against the amount of dispersion pre-compensation for 10-, 28-, and 50-Gbaud signals in Fig. 2. We assume that signals with ideal Nyquist spectra are propagated through one 80-km span of SSMF. Throughout this paper, we model SSMF as having 0.2 dB/km attenuation, 16 ps/nm/km dispersion, and a nonlinear coefficient of 1.3 rad/W/km. The resulting residual distortion is normalised to the maximum value for each symbol rate to illustrate the impact of optimizing the dispersion pre-compensation. For the 10 Gbaud signal, the residual nonlinear distortion with the optimum amount of dispersion pre-compensation is about 0.2% of the maximum value. This means that for low symbol rates, there is an optimal amount of dispersion pre-compensation where a PSA almost ideally cancels the first-order nonlinear distortion. However, optimizing the dispersion pre-compensation has less impact on 28- and 50-Gbaud signals, meaning that residual nonlinear distortions are still present despite the optimization efforts. This indicates that the NLC provided by a PSA becomes less effective as the symbol rate increases.

As a more general method of compensating the residual nonlinear distortion, we propose applying a Volterra nonlinear equalizer (VNLE) with fixed taps at the receiver. In general, an N^{th}-order approximation of the nonlinear perturbation is equivalent to a Volterra-series transfer function including the first 2N+1 Volterra kernels [37]. Previous studies have used this relationship to show that VNLEs based on the inverse of the Volterra-series transfer function are a relatively simple way to mitigate the distortions from fiber nonlinearity [7,9]. Further, increasing the number of terms in the nonlinear perturbation improves accuracy [38], and compensating these terms requires the use of higher-order Volterra kernels. While a VNLE can include kernels of arbitrary order, the complexity of calculating higher-order Volterra kernels grows rapidly [39]. Therefore, VNLEs generally only include the first- and third-order Volterra kernels, which compensate up to the first-order approximation of the nonlinear perturbation, thereby limiting their effectiveness.

In a regular frequency-domain VNLE, the first-order kernel, K_1, compensates the attenuation and dispersion introduced by the fiber link, while the third-order kernel, K_3, governs the nonlinear response of the VNLE [7]. However, when both dispersion and fiber attenuation are compensated optically, like in the copier-PSA scheme, we can set $K_1 = 1$. Additionally, in a link with in-line PSAs, part of the nonlinear distortion has already been compensated and the purpose of the VNLE is to remove only the residual nonlinear distortion. Therefore, we propose using a modified

Optics EXPRESS

VNLE based on the inverse Volterra-series transfer function:

$$E_s(\omega_k, z - L_{\text{link}}) = E_s(\omega_k, z) + A_{\text{NL}}(\omega_k, z - L_{\text{link}}) \tag{14}$$

$$A_{\text{NL}}(\omega_k, z - L_{\text{link}}) = -j\gamma N_{\text{span}} \int\int K_{3,\text{PSA}} E_s(\omega_1, z) E_s^*(\omega_2, z) E_s(\omega - \omega_1 + \omega_2, z) d\omega_1 d\omega_2, \tag{15}$$

where $L_{\text{link}} = N_{\text{span}} L_{\text{span}}$ is the length of the link, and $K_{3,\text{PSA}} = \eta_{\text{res}}(\Delta\Omega, L_{\text{span}})$ is the modified third-order kernel that mitigates only the residual nonlinear distortions. This approach should compensate the first-order residual nonlinear distortions for a wide range of dispersion pre-compensation values and signal bandwidths, assuming that the VNLE has access to the total electric field at the receiver.

3. Numerical simulations

3.1. Simulation setup

To verify the effectiveness of our proposed VNLE, we used numerical simulations to compare the transmission performance of links using phase-sensitive and phase-insensitive in-line optical amplifiers. The block diagram for the simulation setup using in-line PSAs is shown in Fig. 3(a). We generated the idler by taking the phase conjugate of the signal in the 'copier' block, and propagated the signal and idler through a link consisting of 80-km spans of SSMF. As in Section 2, the SSMF had 0.2 dB/km attenuation, 16 ps/nm/km dispersion, and a nonlinear coefficient, γ, of 1.3 rad/W/km. Propagation was modelled by solving the scalar NLSE using the split-step Fourier method. We assumed that there was no nonlinear interaction between the signal and idler, and so used separate split-step solvers. We also used the same SSMF parameters for both signal and idler to maximize the potential impact of NLC using in-line PSAs. To more accurately mimic the experimental setup in Section 4, we added a lumped loss of 18 dB after each span using a variable optical attenuator (VOA). The signal and idler at the output of the span were then amplified using the simplified PSA shown in Fig. 3(b). First, both signal and idler were amplified using optical amplifiers with 1-dB NF. Copies of the signal and idler were then rotated relative to each other by θ_{PLL} and then coherently added. The value of θ_{PLL} was set to maximise the total output power, which emulates the process of tuning the pump phase to maximize the signal gain using a phase-locked loop (PLL) [29]. This model is a direct implementation of Eq. (5), and has been used to emulate PSAs in previous numerical studies [29,30,32]. For the simulations using phase-insensitive amplifiers (PIAs), we used the system in Fig. 3(c), which is the same as Fig. 3(a) with only the signal portion. In this case, the optical amplifier had an NF of 4 dB.

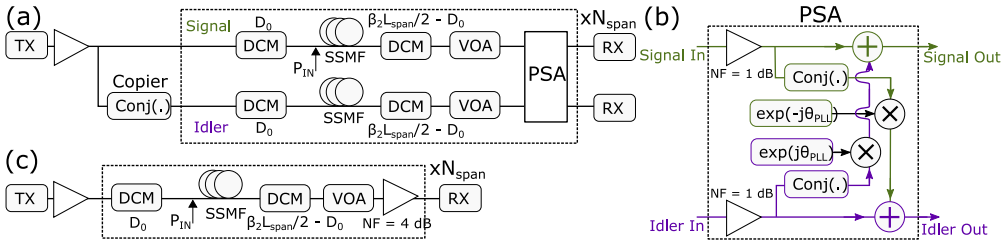

Fig. 3. (a) Block diagram of the numerical simulation for long-haul transmission using a copier-PSA scheme with in-line PSAs. (b) Block diagram of a simplified PSA, assuming high parametric gain and an undepleted pump. (c) Block diagram of the numerical simulation for long-haul transmission using in-line PIAs.

Optics EXPRESS

We considered the transmission of 10-, 28-, and 50-Gbaud single-polarization signals modulated with either quadrature-phase-shift keying (QPSK) or 16QAM. Signals were shaped using root-raised cosine (RRC) filtering with 1% roll-off, and represented in the optical domain using 16 samples per symbol. We assumed that all lasers had zero linewidth.

After transmission, the signals were converted back to the electrical domain and down-sampled to two samples per symbol. The VNLE, if used, was then applied at this point. For links using PIAs, we used a third-order Volterra kernel based on Eq. (11), while for links using PSAs, the modified kernel based on Eq. (14) was implemented. In all cases, we used a frequency-domain VNLE [7] with a block size of 128, and took the necessary fiber parameters directly from the simulation. After this, a two-stage dynamic equalizer was applied; the first stage was used the constant modulus algorithm (CMA) to pre-converge the taps for a decision-directed (DD) stage [40]. We then perform carrier phase estimation using the blind-phase search (BPS) algorithm [41], and then assessed the signal quality.

3.2. Simulation results

To investigate how effectively the modified VNLE can mitigate residual nonlinear distortions, we performed two numerical broad studies. The first study investigated how well the VNLE reduced the residual nonlinear distortion when varying the amount of dispersion pre-compensation. In this case, we fixed the signal launch power, P_{IN}, at 6 dBm and considered transmission through three 80-km spans. We simulated patterns with 2^{12} symbols for each combination of modulation format and symbol rate, and evaluated the performance based on the error vector magnitude using [42]:

$$Q_{\mathrm{EVM}}[\mathrm{dB}] = 10\log_{10}\frac{\sum_{n=1}^{N}|S_{\mathrm{TX}}[n]|^2}{\sum_{n=1}^{N}|S_{\mathrm{TX}}[n]-S_{\mathrm{RX}}[n]|^2}, \tag{16}$$

where $S_{\mathrm{TX}}[n]$ and $S_{\mathrm{RX}}[n]$ are the normalized complex amplitudes of the nth symbol of the transmitted and received signals, respectively, and N is the total number of symbols in the pattern. We should clarify that we use Q_{EVM} in this context to estimate the relative performance of the systems under investigation, and that the values do not map directly to the bit-error ratio (BER).

Figure 4 plots Q_{EVM} vs dispersion pre-compensation for signals with different symbol rates. Circular markers are used for the QPSK signals, while square markers are used for the 16QAM signals. In all cases, adjusting the amount of dispersion pre-compensation affects performance, and Q_{EVM} is higher for PSA links (blue markers) compared to PIA links (red markers). For PSA links without the VNLE (filled markers), there is a large difference in Q_{EVM} between the best and worst values of dispersion pre-compensation, highlighting that nonlinearity mitigation using in-line PSAs is very sensitive to link design. Further, the optimum amount of dispersion pre-compensation was the same for QPSK and 16QAM signals, suggesting modulation format independence.

Applying our modified VNLE to the link with in-line PSAs (open markers) increases Q_{EVM} for sub-optimal links, which indicates that it can compensate residual nonlinear distortions for a broad range of dispersion pre-compensation settings. For the links with 10 Gbaud signals, using the VNLE does not increase the maximum Q_{EVM}. This indicates that there is negligible residual nonlinear distortions at that operating point. However, the VNLE does increases the maximum Q_{EVM} for links with 28- and 50-Gbaud signals, suggesting that there are still residual nonlinear distortions after the dispersion pre-compensation has been optimized. These trends are the same for both modulation formats. Overall, these simulation results are consistent with the predictions of the perturbation analysis in Section 2.

Our second numerical study was aimed at estimating how combining our modified VNLE with in-line PSAs affects the maximum transmission distance at the optimum launch power. In this case, we simulated patterns with 2^{16} symbols, and found the distance when BER $\leq 10^{-3}$. For both PIA and PSA links, we optimized the amount of dispersion pre-compensation using

Optics EXPRESS

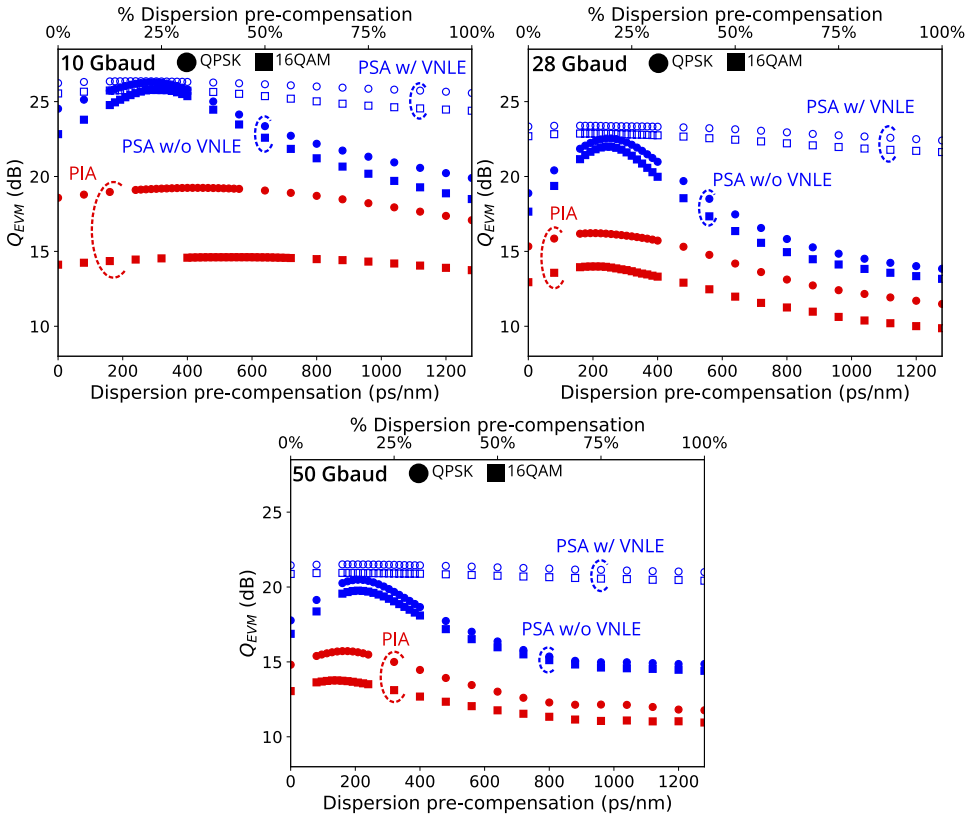

Fig. 4. Simulated Q_{EVM} vs. dispersion pre-compensation after three spans for QPSK and 16QAM signals at 10-, 28-, and 50-Gbaud, for links employing PIAs, PSAs, and PSAs with a VNLE. P_{IN} was fixed at 6 dBm

the results in Fig. 4. We also simulated a PIA link with 6-dB lower span loss, and a PSA link with 100% dispersion pre-compensation. The 'low loss' PIA link was designed to achieve the same transmission distance as a link with in-line PSAs at low launch powers. This provides an estimate for how the low-noise amplification property of PSAs increases the system reach. We can then attribute longer transmission distances to the nonlinearity mitigation provided by in-line PSAs. We used the same value of dispersion pre-compensation for both PIA links. On the other hand, the PSA link with 100% dispersion pre-compensation is of interest because we would no longer need the DCM placed after the fiber span. This would reduce the overall span loss but increase the residual nonlinear distortion, which allows us to explore the trade-off between span loss and nonlinearity mitigation, and how this trade-off changes with the addition of a VNLE.

We plot the maximum transmission distance against launch power for all six combinations of symbol rate and modulation format in Fig. 5. For each link, we consider the performance with (open markers) and without (filled markers) a VNLE using the appropriate third-order kernel. The dashed lines are provided as guides for the eye. At low launch powers, the links using PSAs and the low-loss PIA link exhibit a 4-times reach improvement relative to the reference PIA case, as expected from improved linear performance. Comparing the two links using in-line PIAs, reducing the span loss by 6 dB doubles the maximum transmission distance for all 6 simulated systems. Therefore we attribute any reach improvements beyond a factor of two to the nonlinearity mitigation provided by the in-line PSAs. Additionally, while using a VNLE improves

Optics EXPRESS

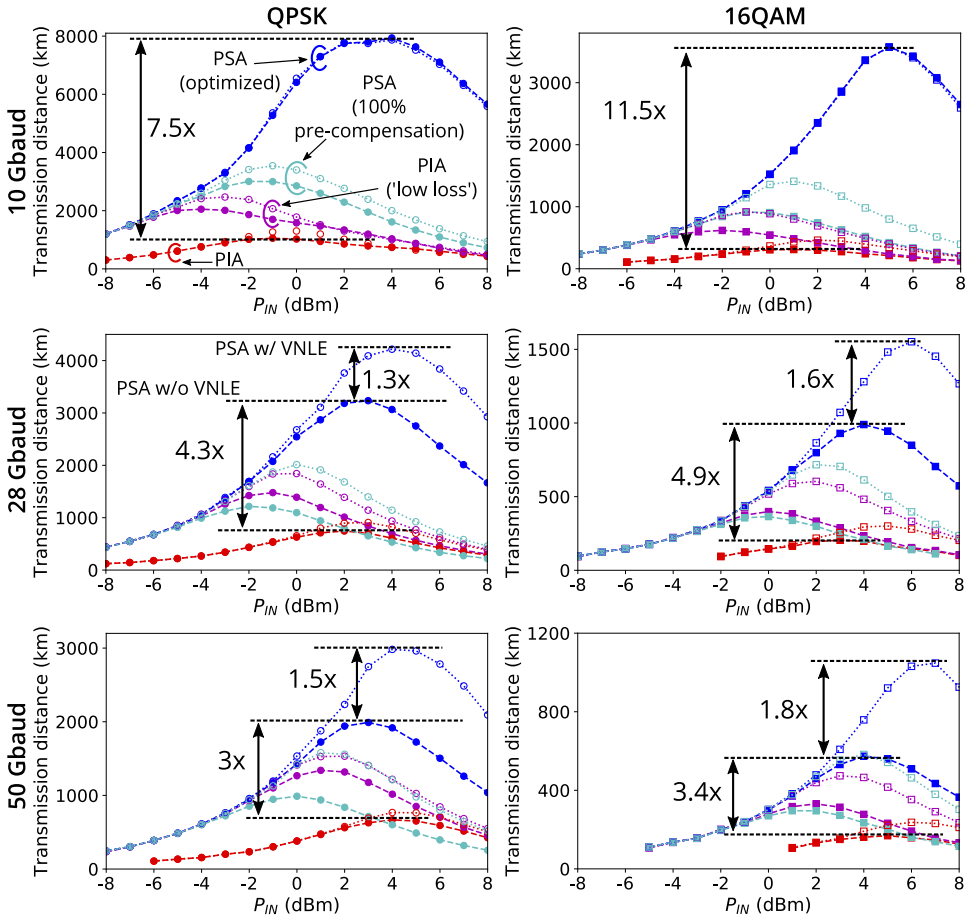

Fig. 5. Simulated maximum transmission distance (for BER $\leq 10^{-3}$) vs. launch power for QPSK (left) and 16QAM (right) at 10- (top), 28- (center), and 50-Gbaud (bottom) signals.

the maximum transmission distance of both PIA links, even longer transmission distances can be achieved by employing in-line PSAs.

Comparing the reach of the link with in-line PSAs and the optimized value of dispersion pre-compensation with the reach of the reference PIA link at 10 Gbaud, PSAs enable a reach improvement of around 7.5 for a QPSK-modulated signal and 11.5 for a signal with 16QAM. Applying the VNLE does not improve performance in this case, indicating that there is no residual nonlinear distortion. As the symbol rate increases, however, the reach improvement enabled by PSAs decreases. At 28 Gbaud, the QPSK signal experiences a 4.3-times reach improvement using in-line PSAs while the 16QAM improvement is reduced to 4.9; at 50 Gbaud in-line PSAs increase the reach of a QPSK signal by a factor of 3 and of a 16QAM signal by a factor of 3.4. This shows that PSAs by themselves cannot fully compensate the nonlinear distortion, leading to a larger residual nonlinear distortion as the optical bandwidth increases. When our modified VNLE is applied to the 28- and 50-Gbaud signals, the maximum transmission distance increases due to the mitigation of the residual nonlinear distortion. For the 28-Gbaud QPSK signal, using a VNLE in combination with in-line PSAs enables 30% longer reach compared to only PSAs, while for the 28-Gbaud 16QAM signal, the reach increase is 60%. The impact of the VNLE is even larger for 50-Gbaud signals: the transmission distance is increased by about 50% for

Optics EXPRESS

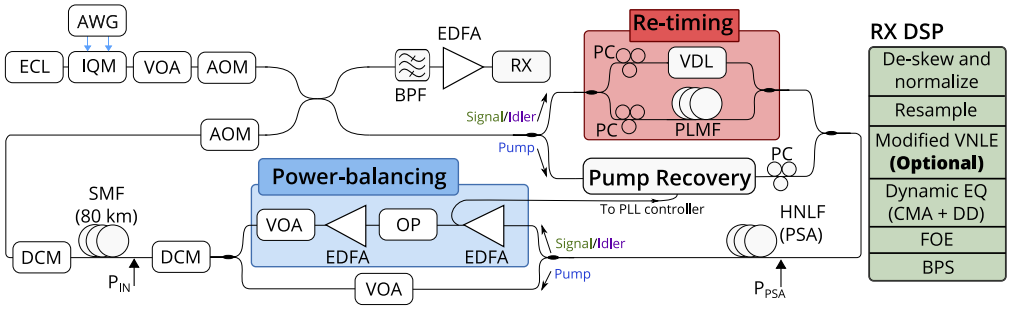

Fig. 6. Block diagram of experimental setup for re-circulating loop experiment using copier-PSA scheme. Inset: Receiver DSP flow-chart. Abbreviations are explained in the text.

QPSK modulation, and 80% for 16QAM. This confirms that our modified VNLE can mitigate the accumulated residual distortion experienced by a range of signals, thereby improving overall link performance.

Compared to the link with in-line PSAs and optimized dispersion pre-compensation, using in-line PSAs with 100% dispersion pre-compensation results in significantly shorter reach. Without applying the VNLE, this is expected as sub-optimal link design results in a larger residual nonlinear distortion. However, PSA systems with 100% dispersion pre-compensation and a VNLE achieve roughly half of the maximum transmission distance of the same system with optimized dispersion pre-compensation and a VNLE. We believe that this is because using sub-optimal dispersion pre-compensation increases the residual distortion in every span, and so the signal can traverse fewer spans before the distortion becomes too large for the VNLE to compensate. From the PIA simulations we discussed earlier, reducing the span loss by 6 dB roughly doubles the system reach. Therefore, if the insertion loss of the post-compensation DCM is less than 6 dB, this result indicates that it is better to optimize the dispersion pre-compensation than to remove the DCM. This conclusion does not change when our modified VNLE is used.

4. Experimental verification

4.1. Experimental setup

To verify our simulation results, we performed a proof-of-concept experiment using the re-circulating loop setup shown in Fig. 6. We generated a 10-Gbaud 16QAM signal that was digitally filtered using an RRC filter with 0.1 roll-off, and stored it on an arbitrary waveform generator (AWG) with 25 GHz electrical bandwidth and 60 GSa/s digital-to-analogue converters. The signal was then modulated onto an external cavity laser (ECL) centered at a wavelength of 1550.1 nm using an IQ modulator (IQM) with 20 GHz electrical bandwidth. The linewidth of the ECL was less than 100 kHz. A VOA set the power of the signal launched into a re-circulating loop that was controlled using two acousto-optic modulators (AOMs).

The first stage in the loop was a re-timing and polarization control stage followed by a four-spool cascade of highly nonlinear fiber (HNLF). The zero-dispersion wavelength of the HNLF cascade was 1544 nm. In the first pass through the loop, only the signal and pump were present, and so the HNLF cascade acted as a 'copier' to generate the idler wave. For all future passes through the loop, the HNLF cascade operated as a PSA. Polarization controllers (PCs) aligned the state of polarization of the signal, pump, and idler to maximise the parametric gain. After the HNLF cascade, the high-power pump, centered at 1554.1 nm, was separated from the signal and idler, and attenuated to −1.5 dBm for transmission through the fiber span. In the next pass through the loop, the pump was recovered from this pilot tone using optical injection locking, and a

Optics EXPRESS

piezo-controlled fiber stretcher with a PLL control circuit adjusted the phase of the pump to maximize the gain of the PSA [23]. At the input of the HNLF cascade, the pump power was 29.7 dBm. In the signal/idler path, an optical processor (OP) ensured that the signal and idler were launched into the span with the same power, and an EDFA followed by a VOA controlled the signal launch power into the span (P_{IN}). Channelized DCMs employing fiber-Bragg grating technology were placed before and after the 80-km span of single-mode fiber (SMF) to provide dispersion pre- and post-compensation. As the DCMs did not undo the walk-off between the signal and idler, path-length matching fiber (PLMF) and a variable optical delay line (VDL) were used to temporally align the signal and idler into the PSA. We measured the loss between P_{IN} and P_{PSA} as 34 dB. After each pass through the span, part of the light was coupled out of the loop, and the signal was de-multiplexed using an optical band-pass filter (BPF) before being coherently detected. The electrical waveforms were then captured using a 50-GSa/s real-time oscilloscope with 33-GHz electrical bandwidth, and stored for offline processing. Note that because the signal was coupled out of the loop before the HNLF cascade, the nonlinear distortion from the final span was not mitigated using a PSA.

The receiver DSP structure is shown on the right of Fig. 6. The electro-optic response of the receiver was compensated and the electrical signal was normalized before being down-sampled to two samples per symbol. The modified VNLE, if used, was then applied after scaling the received signal so that its average power was equal to the nominal value of P_{IN}. For all measurements, we used a static frequency-domain VNLE [7] with a block size of 32, and the modified third-order kernel given by Eq. (14). The modified third-order kernel assumed that each 80-km span of fiber had 0.2 dB/km attenuation, 16 ps/nm/km dispersion, and a nonlinear coefficient of 1.3 rad/W/km. The value of D_0 used by the VNLE corresponded to the dispersion applied by the DCM placed before the span. Linear equalization was accomplished using a two-stage dynamic equalizer where a CMA stage was used to pre-converge the taps for a DD stage. Frequency offset estimation (FOE) between the signal and local oscillator was performed by taking the fourth-power of the spectrum, and the BPS algorithm was used to compensate laser phase noise. Finally, the signal performance was assessed by directly counting the number of bit errors, and the BER was converted to Q using $Q_{\mathrm{BER}}[\mathrm{dB}] = 20\log_{10}(\sqrt{2}\mathrm{erfc}^{-1}(2 \times \mathrm{BER}))$. Note that a 1-dB increase in Q_{BER} is roughly equivalent to a 1-dB increase in Q_{EVM}. We used the QAMpy package [43] for all DSP functions besides the VNLE.

4.2. Experimental results

Figure 7(a) plots Q_{BER} with (open markers) and without (close markers) our modified VNLE against the amount of dispersion pre-compensation after 10 spans. In this case, P_{IN} is fixed at 4 dBm, which is slightly larger than the optimum launch power for this system (see Fig. 7(b)). Without the VNLE, applying 323 ps/nm dispersion pre-compensation enables the best performance, and moving away from this value incurs a performance penalty. Fully pre-compensating the span results in the worst performance. When using our modified VNLE, performance is generally improved for sub-optimal amounts of dispersion pre-compensation, with Q_{BER} increasing by about 2 dB at both 0% and 100% pre-compensation. However, the VNLE does not improve performance close to the best dispersion pre-compensation setting, and in some cases causes a small penalty. These trends are broadly consistent with the simulation results and our perturbation analysis. We believe that the performance penalty originates from using an imperfect estimate of the fiber parameters in the fixed-tap VNLE; because the residual nonlinear distortion is small for that operating point, the error introduced by an imperfect Volterra kernel when calculating the residual distortion may be larger than the residual nonlinear distortion itself. Employing a VNLE with adaptive taps (e.g., [44]) should reduce this penalty, though it would increase the computational complexity.

Optics EXPRESS

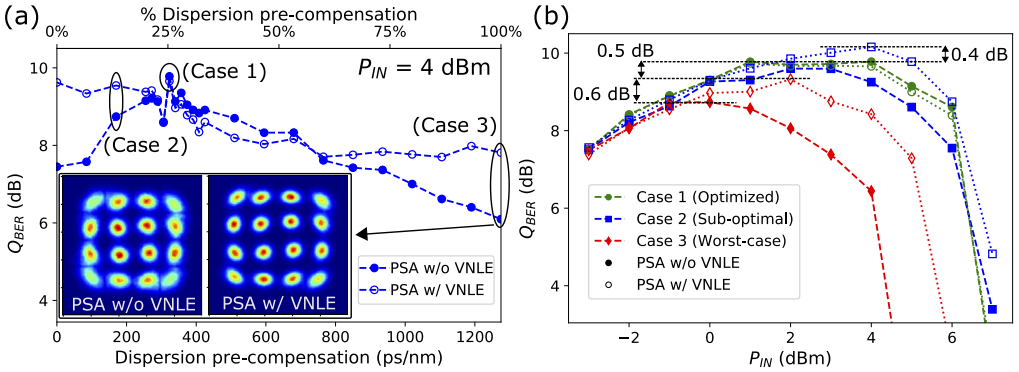

Fig. 7. (a) Experimental measurement of Q_{BER} vs. dispersion pre-compensation for a 10-Gbaud 16QAM signal after 10 spans with and without the VNLE. Inset: Measured constellations with and without the VNLE with 100% pre-compensation. (b) Q_{BER} vs. P_{IN} for: 323 ps/nm (Case 1), 170 ps/nm (Case 2), or 1280 ps/nm (Case 3) dispersion pre-compensation, with and without the VNLE.

In the inset of Fig. 7(a), we plot constellation diagrams with and without the VNLE for 1275 ps/nm (100%) pre-compensation. Without the VNLE (left), the residual nonlinear distortion is clearly visible on the outer points. This distortion is reduced significantly by the VNLE (right), which confirms the effectiveness of our proposed VNLE.

Figure 7(b) plots Q_{BER} vs P_{IN} for three different values of dispersion pre-compensation, marked on Fig. 7(a), with and without a VNLE. Case 1 applied 323 ps/nm pre-compensation, which enabled the best performance without a VNLE. Case 2 applied 170 ps/nm pre-compensation, and was investigated because it was a slightly sub-optimal setting. Case 3 fully pre-compensated the span (1275 ps/nm), which Fig. 7(a) indicated was the worst case. Using our proposed VNLE improves Q_{BER} at the optimum launch power for Cases 2 and 3. In fact, combining the link design of Case 2 with the VNLE has 0.4 dB higher Q_{BER} than Case 1 without the VNLE. While the simulations in Section 3 indicate that a VNLE should not improve the performance of a 10-Gbaud 16QAM signal, the design of the re-circulating loop meant that the nonlinear distortion in the last span was not cancelled by a PSA. Therefore, we attribute this small improvement to the VNLE mitigating part of the nonlinear distortion in the last span. Additionally, the performance penalty between Case 3 and Case 1 is reduced from 1.1 dB to 0.5 dB when the VNLE is used. However, as in Fig. 7(a), the VNLE caused a small penalty when the dispersion pre-compensation was optimized. These results confirm that a post-compensation VNLE can mitigate the residual distortion left after imperfect nonlinearity mitigation using a PSA.

5. Discussion

In the analysis presented in Section 2, we made three key assumptions. First, we only considered links where PSAs were used as lumped amplifiers. This is sub-optimal for NLC using coherent addition [27]. Therefore, previous numerical [30] and experimental [31] investigations have studied how the use of Raman amplification could improve nonlinearity compensation using in-line PSAs. The impact of Raman amplification can be accounted for by including a distance-dependent gain term in Eq. (11), though a complete analysis of that system is beyond the scope of this paper. Additionally, the system will be dominated by noise from the Raman amplification and so performing low-noise amplification using PSAs will have negligible benefit [26]. Therefore, combining Raman amplification and in-line PSAs is similar to transmitting PCTW signals over a Raman-amplified link. While there may be some benefits to performing NLC after every span

Optics EXPRESS

rather than at the end of the link [45], the complexity of deploying in-line PSAs should also be considered when comparing these two systems.

Our second and third assumptions were that dispersion was fully compensated in each span, and that the amount of dispersion pre-compensation was the same in every span. This combination can often result in poor transmission performance since the nonlinear distortion from each span adds in-phase [34]. As a result, it is possible that the simulation results in Section 3 are artificially poor for links using phase-insensitive amplifiers, which enhances the relative benefit of using in-line PSAs. However, the main focus of this paper is the residual nonlinear distortion in links with in-line PSAs, and how this residual distortion changes with the symbol rate and modulation format. Therefore, sub-optimal performance for phase-insensitive amplifier links should not dramatically affect our main conclusions. Additionally, while fully compensating the dispersion after every span is required when using PSAs, the amount of dispersion pre-compensation does not have to be the same in each span. As such, our perturbation approach could be used to design a link where the amount of dispersion pre-compensation changes between spans in order to reduce how quickly the residual distortion accumulates. A basic implementation of this approach was recently investigated by Astra *et al.* [32] using exhaustive numerical simulations. Further, the reach improvement reported in [32] after jointly optimizing the dispersion pre-compensation over several spans is larger than what we accomplished with our modified VNLE. This suggests that optimizing the link design to reduce how quickly the residual nonlinear distortions accumulate may be better than relying on DSP to compensate a large accumulated distortion at the receiver. As this affects the signal in the optical domain, it also overcomes the limitations imposed by the electrical bandwidth of the receiver, which becomes important when considering wavelength division multiplexed signals.

Finally, we should point out that there are inconsistencies between our simulations and previously reported experimental results. Specifically, our simulation results in Section 3 predict that 16QAM signals should benefit more from the use of in-line PSAs than QPSK signals, but the experimental demonstration using QPSK in [23] reported a larger reach extension from PSAs than the demonstration on the same setup using a 16QAM signal in [46]. However, previous single-span experimental results indicate that PSAs can provide better nonlinearity mitigation for 16QAM signals as opposed to QPSK signal (compare [22] with [29]), which is consistent with our simulations. Given these data, we believe that there is an experimental issue when transmitting 16QAM in a re-circulating loop, e.g., an imperfect PLL would increase the impact of the level-dependent gain [29], and this penalty could grow with multiple trips through the loop. The exact reason for the difference between simulation and experimental results requires further investigation. However, the fact that our VNLE improves performance despite the imperfections with our experiment suggests that our approach is conceptually sound, even if the numerical simulations do not perfectly match the experimental results.

6. Conclusion

In conclusion, this paper has presented an extensive investigation of nonlinearity mitigation using PSAs. By combining first-order perturbation theory with the matrix description of parametric amplifiers, we have shown mathematically that links using in-line PSAs for lumped amplification have a residual nonlinear distortion. The existence of this residual nonlinear distortion is the underlying reason why nonlinearity mitigation using PSAs depends on the link parameters and signal bandwidth, as described in Eq. (14). We then proposed and evaluated a modified third-order VNLE as a way to mitigate residual nonlinear distortions. We numerically simulated links with several combinations of symbol rate, modulation format, and dispersion pre-compensation, and showed that using our modified VNLE reduces the residual nonlinear distortion in all tested scenarios. Compensating the residual nonlinear distortion can increase the maximum transmission distance of a link employing in-line PSAs by up to 80%. In a proof-of-concept

Optics EXPRESS

experiment, we transmitted a 10-Gbaud 16QAM signal through a 10×80-km link with in-line PSAs, and demonstrated that our proposed VNLE reduced the dependence on the amount of dispersion pre-compensation and enabled a 0.4-dB increase in the maximum Q_{BER}. Finally, we note that designing the link to minimize the accumulation of the residual nonlinear distortion [32] may be more effective than digitally compensating the residual distortion at the end of the link. In this scenario, the analysis presented in Section 2 can be used to efficiently extend the optimization strategy outlined in [32] to entire long-haul links.

Funding

Swedish Research Council (VR) (2015-00535).

References

1. P. P. Mitra and J. B. Stark, "Nonlinear limits to the information capacity of optical fibre communications," Nature **411**(6841), 1027–1030 (2001).
2. R.-J. Essiambre, G. J. Foschini, G. Kramer, and P. J. Winzer, "Capacity limits of information transport in fiber-optic networks," Phys. Rev. Lett. **101**(16), 163901 (2008).
3. A. Ellis, J. Zhao, and D. Cotter, "Approaching the non-linear Shannon limit," J. Lightwave Technol. **28**(4), 423–433 (2010).
4. C. E. Shannon, "A mathematical theory of communication," Bell Syst. Tech. J. **27**(3), 379–423 (1948).
5. G. Agrawal, *Nonlinear Fiber Optics* (Academic, 2013).
6. E. Ip, "Nonlinear compensation using backpropagation for polarization-multiplexed transmission," J. Lightwave Technol. **28**(6), 939–951 (2010).
7. F. P. Guiomar and A. N. Pinto, "Simplified Volterra series nonlinear equalizer for polarization-multiplexed coherent optical systems," J. Lightwave Technol. **31**(23), 3879–3891 (2013).
8. R. Dar and P. Winzer, "Nonlinear interference mitigation: Methods and potential gain," J. Lightwave Technol. **35**(4), 903–930 (2017).
9. J. C. Cartledge, F. P. Guiomar, F. R. Kschischang, G. Liga, and M. P. Yankov, "Digital signal processing for fiber nonlinearities [invited]," Opt. Express **25**(3), 1916–1936 (2017).
10. R. A. Fisher, B. R. Suydam, and D. Yevick, "Optical phase conjugation for time-domain undoing of dispersive self-phase-modulation effects," Opt. Lett. **8**(12), 611–613 (1983).
11. M. Morshed, L. B. Du, B. Foo, M. D. Pelusi, B. Corcoran, and A. J. Lowery, "Experimental demonstrations of dual polarization CO-OFDM using mid-span spectral inversion for nonlinearity compensation," Opt. Express **22**(9), 10455–10466 (2014).
12. S. Kumar and D. Yang, "Optical backpropagation for fiber-optic communications using highly nonlinear fibers," Opt. Lett. **36**(7), 1038–1040 (2011).
13. R. Stolen and J. Bjorkholm, "Parametric amplification and frequency conversion in optical fibers," IEEE J. Quantum Electron. **18**(7), 1062–1072 (1982).
14. M. Karlsson, "Transmission systems with low noise phase-sensitive parametric amplifiers," J. Lightwave Technol. **34**(5), 1411–1423 (2016).
15. R. Slavík, F. Parmigiani, J. Kakande, C. Lundström, M. Sjödin, P. A. Andrekson, R. Weerasuriya, S. Sygletos, A. D. Ellis, L. Grüner-Nielsen, D. Jakobsen, S. Herstrøm, R. Phelan, J. O'Gorman, A. Bogris, D. Syvridis, S. Dasgupta, P. Petropoulos, and D. J. Richardson, "All-optical phase and amplitude regenerator for next-generation telecommunications systems," Nat. Photonics **4**(10), 690–695 (2010).
16. A. Lorences-Riesgo, L. Liu, S. L. I. Olsson, R. Malik, A. Kumpera, C. Lundström, S. Radic, M. Karlsson, and P. A. Andrekson, "Quadrature demultiplexing using a degenerate vector parametric amplifier," Opt. Express **22**(24), 29424–29434 (2014).
17. B. Zheng, Q. Xie, and C. Shu, "Raman-assisted phase-sensitive amplification enabled optical add-drop filter," IEEE Photonics Technol. Lett. **29**(23), 2047–2050 (2017).
18. C. M. Caves, "Quantum limits on noise in linear amplifiers," Phys. Rev. D: Part. Fields **26**(8), 1817–1839 (1982).
19. Z. Tong, C. Lundström, P. A. Andrekson, C. J. McKinstrie, M. Karlsson, D. J. Blessing, E. Tipsuwannakul, B. J. Puttnam, H. Toda, and L. Grüner-Nielsen, "Towards ultrasensitive optical links enabled by low-noise phase-sensitive amplifiers," Nat. Photonics **5**(7), 430–436 (2011).
20. M. Asobe, T. Umeki, and O. Tadanaga, "Phase sensitive amplification with noise figure below the 3 dB quantum limit using CW pumped PPLN waveguide," Opt. Express **20**(12), 13164–13172 (2012).
21. R. Tang, J. Lasri, P. S. Devgan, V. Grigoryan, P. Kumar, and M. Vasilyev, "Gain characteristics of a frequency nondegenerate phase-sensitive fiber-optic parametric amplifier with phase self-stabilized input," Opt. Express **13**(26), 10483–10493 (2005).
22. B. Corcoran, M. Karlsson, C. Lundström, S. Olsson, and P. Andrekson, "Mitigation of nonlinear impairments on QPSK data in phase-sensitive amplified links," in *39th European Conference and Exhibition on Optical Communication (ECOC 2013)*, (Institution of Engineering and Technology, 2013), pp. 1–3.

Optics EXPRESS

23. S. L. I. Olsson, H. Eliasson, E. Astra, M. Karlsson, and P. A. Andrekson, "Long-haul optical transmission link using low-noise phase-sensitive amplifiers," Nat. Commun. **9**(1), 2513 (2018).
24. C. J. McKinstrie, S. Radic, and M. G. Raymer, "Quantum noise properties of parametric amplifiers driven by two pump waves," Opt. Express **12**(21), 5037–5066 (2004).
25. Z. Tong, A. Bogris, M. Karlsson, and P. A. Andrekson, "Full characterization of the signal and idler noise figure spectra in single-pumped fiber optical parametric amplifiers," Opt. Express **18**(3), 2884–2893 (2010).
26. B. Corcoran, R. Malik, S. L. I. Olsson, C. Lundström, M. Karlsson, and P. A. Andrekson, "Noise beating in hybrid phase-sensitive amplifier systems," Opt. Express **22**(5), 5762–5771 (2014).
27. X. Liu, A. R. Chraplyvy, P. J. Winzer, R. W. Tkach, and S. Chandrasekhar, "Phase-conjugated twin waves for communication beyond the Kerr nonlinearity limit," Nat. Photonics **7**(7), 560–568 (2013).
28. X. Liu, S. Chandrasekhar, P. J. Winzer, R. W. Tkach, and A. R. Chraplyvy, "Fiber-nonlinearity-tolerant superchannel transmission via nonlinear noise squeezing and generalized phase-conjugated twin waves," J. Lightwave Technol. **32**(4), 766–775 (2014).
29. S. L. I. Olsson, B. Corcoran, C. Lundström, T. A. Eriksson, M. Karlsson, and P. A. Andrekson, "Phase-sensitive amplified transmission links for improved sensitivity and nonlinearity tolerance," J. Lightwave Technol. **33**(3), 710–721 (2015).
30. H. Eliasson, S. L. I. Olsson, M. Karlsson, and P. A. Andrekson, "Mitigation of nonlinear distortion in hybrid Raman/phase-sensitive amplifier links," Opt. Express **24**(2), 888–900 (2016).
31. H. Eliasson, K. Vijayan, B. Foo, S. L. I. Olsson, E. Astra, M. Karlsson, and P. A. Andrekson, "Phase-sensitive amplifier link with distributed Raman amplification," Opt. Express **26**(16), 19854–19863 (2018).
32. E. Astra, H. Eliasson, T. Ruuben, and P. A. Andrekson, "Improved mitigation of self-phase modulation induced impairments in 28 GBaud phase-sensitive amplified links," Opt. Express **27**(4), 4304–4316 (2019).
33. K. Vijayan, H. Eliasson, B. Foo, S. L. I. Olsson, M. Karlsson, and P. A. Andrekson, "Optical bandwidth dependency of nonlinearity mitigation in phase-sensitive amplifier links," in *European Conference on Optical Communications 2018*, (2018), pp. 1–3.
34. H. Louchet, A. Hodzic, K. Petermann, A. Robinson, and R. Epworth, "Simple criterion for the characterization of nonlinear impairments in dispersion-managed optical transmission systems," IEEE Photonics Technol. Lett. **17**(10), 2089–2091 (2005).
35. G. Saavedra, G. Liga, and P. Bayvel, "Volterra-assisted optical phase conjugation: A hybrid optical-digital scheme for fiber nonlinearity compensation," J. Lightwave Technol. **37**(10), 2467–2479 (2019).
36. B. Foo, M. Karlsson, K. Vijayan, M. Mazur, and P. A. Andrekson, "Combining phase-sensitive amplifiers with DSP for enhanced nonlinearity mitigation," in *2019 European Conference on Optical Communications*, (Institution of Engineering and Technology, 2019), pp. 1–3. (to be published).
37. A. Vannucci, P. Serena, and A. Bononi, "The RP method: a new tool for the iterative solution of the nonlinear Schrödinger equation," J. Lightwave Technol. **20**(7), 1102–1112 (2002).
38. S. Kumar and D. Yang, "Second-order theory for self-phase modulation and cross-phase modulation in optical fibers," J. Lightwave Technol. **23**(6), 2073–2080 (2005).
39. K. Peddanarappagari and M. Brandt-Pearce, "Volterra series transfer function of single-mode fibers," J. Lightwave Technol. **15**(12), 2232–2241 (1997).
40. M. S. Faruk and S. J. Savory, "Digital signal processing for coherent transceivers employing multilevel formats," J. Lightwave Technol. **35**(5), 1125–1141 (2017).
41. T. Pfau, S. Hoffmann, and R. Noé, "Hardware-efficient coherent digital receiver concept with feedforward carrier recovery for *M*-qam constellations," J. Lightwave Technol. **27**(8), 989–999 (2009).
42. R. A. Shafik, M. S. Rahman, and A. R. Islam, "On the extended relationships among EVM, BER and SNR as performance metrics," in *2006 International Conference on Electrical and Computer Engineering*, (IEEE, 2006), pp. 408–411.
43. J. Schröder and M. Mazur, "QAMPy a DSP chain for optical communications," (2018). DOI: 10.5281/zenodo.1195720.
44. F. Zhang, Y. Gao, Y. Luo, J. Li, L. Zhu, L. Li, Z. Chen, and A. Xu, "Experimental demonstration of intra-channel nonlinearity mitigation in coherent QPSK systems with nonlinear electrical equaliser," Electron. Lett. **46**(5), 353–355 (2010).
45. B. Foo, B. Corcoran, and A. J. Lowery, "Distributed nonlinear compensation using optoelectronic circuits," J. Lightwave Technol. **36**(6), 1326–1339 (2018).
46. S. L. I. Olsson, M. Karlsson, and P. A. Andrekson, "Long-haul optical transmission of 16-QAM signal with in-line phase-sensitive amplifiers," in *2017 European Conference on Optical Communication (ECOC)*, (IEEE, 2017), pp. 1–3.